ApJ in press
Preprint typeset using LaTeX style emulateapj v. 6/22/04

EARLY SUPERSYMMETRIC COLD DARK MATTER SUBSTRUCTURE

Jürg Diemand, Michael Kuhlen, & Piero Madau
Department of Astronomy & Astrophysics, University of California, Santa Cruz, CA 95064
ApJ in press

ABSTRACT

Earth-mass "microhalos" may be the first objects to virialize in the early universe. Their ability to survive the hierarchical clustering process as substructure in the larger halos that form subsequently has implications for dark matter detection experiments. We present a large N-body simulation of early substructure in a supersymmetric cold dark matter (SUSY-CDM) scenario characterized by an exponential cutoff in the power spectrum at $M_c = 10^{-6}$ M$_\odot$. The simulation resolves a 0.014 M$_\odot$ parent "SUSY" halo at $z = 75$ with 14 million particles. On these scales the effective index of the power spectrum approaches -3, and a range of mass scales collapse almost simultaneously. Compared to a $z = 0$ galaxy cluster substructure within our SUSY host is less evident both in phase-space and in physical space, and it is less resistant against tidal disruption. As the universe expands by a factor of 1.3, we find that between 20 and 40 percent of well-resolved SUSY substructure is destroyed, compared to only ~ 1 percent in the low-redshift cluster. Nevertheless SUSY substructure is just as abundant as in $z = 0$ galaxy clusters, i.e. the normalized mass and circular velocity functions are very similar. The dark matter self-annihilation γ-ray luminosity from bound subhalos and other deviations from a smooth spherical configuration is at least comparable to the spherically-averaged signal in the SUSY host, and at least three times larger than the spherically-averaged signal in the cluster host. Such components must be taken into account when estimating the total cosmological extragalactic γ-ray annihilation background. The relative contribution of bound substructure alone to the total annihilation luminosity is about four times smaller in the SUSY host than in the $z = 0$ cluster because of the smaller density contrast of sub-microhalos.

Subject headings: methods: N-body simulations – methods: numerical – early universe – structure formation

1. INTRODUCTION

The key idea of the standard cosmological paradigm for the formation of structure in the universe, that primordial density fluctuations grow by gravitational instability driven by cold, collisionless dark matter (CDM), is constantly being elaborated upon and explored in detail through supercomputer simulations, and tested against a variety of astrophysical observations. The leading candidate for dark matter (DM) is the neutralino, a weakly interacting massive particle predicted by the supersymmetry (SUSY) theory of particle physics. While in a SUSY-CDM scenario the mass of bound DM systems (halos) may span about twenty order of magnitudes, from the most massive galaxy clusters down to Earth-mass clumps (e.g. Green, Hofmann, & Schwarz 2004), it is the smallest DM microhalos that collapse first, and only these smallest scales are affected by the nature of the relic DM candidate.

Recent numerical simulations of the collapse of the earliest and smallest gravitationally bound CDM clumps (Diemand, Moore, & Stadel 2005; Gao et al. 2005) have shown that tiny virialized microhalos form at redshifts above 50 with internal density profiles that are quite similar to those of present-day galaxy clusters. At these epochs a significant fraction of neutralino DM has already been assembled into non-linear Earth-mass overdensities. If this first generation of dark objects were to survive gravitational disruption during the early hierarchical merger and accretion process – as well as late tidal disruption from stellar encounters (Zhao et al. 2005; Berezinsky, Dokuchaev, & Eroshenko 2006) – then over 10^{15} such clumps may populate the halo of the Milky Way (Diemand et al. 2005). The nearest microhalos may be among the brightest sources of γ-rays from neutralino annihilation. As the annihilation rate increases quadratically with the DM density, small-scale clumpiness may enhance the total γ-ray flux from nearby extragalactic systems (like M31), making them detectable by the forthcoming *GLAST* satellite or the next-generation of air Cerenkov telescopes (e.g. Oda, Totani, & Nagashima 2005). Dark matter caustics might occur within the first generation of halos. Caustics are not resolved in N-body simulations like the ones discussed here and might have significant effects on DM detection experiments (e.g. Mohayaee & Shandarin 2005).

The possibility of observing the fingerprints of the smallest-scale structure of CDM in direct and indirect DM searches hinges on the ability of microhalos to survive the hierarchical clustering process as substructure within the larger halos that form at later times. In recent years high-resolution N-body simulations have enabled the study of gravitationally-bound subhalos with $M_{\rm subh}/M_{\rm halo} \gtrsim 10^{-6}$ on galaxy (and galaxy cluster) scales (Moore et al. 1999; Klypin et al. 1999; Stoehr et al. 2003; Diemand, Moore, & Stadel 2004; Gao et al. 2004; Reed et al. 2005). The main differences between these subhalos – the surviving cores of objects which fell together during the hierarchical assembly of galaxy-size systems – and the tiny sub-microhalos mentioned above is that on the smallest CDM scale the

Electronic address: diemand@ucolick.org.

effective index of the linear power spectrum of mass density fluctuations is close to -3. In this regime typical halo formation times depend only weakly on halo mass, the capture of small clumps by larger ones is very rapid, and sub-microhalos may be more easily disrupted. Yet previous simulations that have resolved subhalos above 1000 $M_\odot$ down to $z = 4$ (Moore et al. 2001) and above 10 $M_\odot$ down to $z = 49$ (Gao et al. 2005) have found that the substructure abundance in early DM halos is quite similar to that of their present-day counterparts.

In this paper we extend this range further down towards the free-streaming cutoff mass of $10^{-6}\,M_\odot$ by using a mass resolution of $10^{-9}\,M_\odot$ in a large high-resolution N-body simulation of early substructure in SUSY-CDM. The simulation resolves a $0.014\,M_\odot$ host halo at $z = 75$ with 14 million particles within its virial radius. The mass resolution and power spectrum are the same as in one of the runs presented in Diemand et al. (2005), which focused on a region of average density. The new simulation discussed in this work has a high resolution region that covers an eight times larger initial volume [120 (comoving pc)]^3 and is centered on the highest-σ peak of the same 3 comoving kpc parent simulation cube.

The plan of the paper is as follows. In § 2 we describe the initial conditions, numerical methods, and parameters of our simulations. In § 3 we present the properties of our SUSY parent halo and its substructure, comparing them to a low-redshift massive galaxy cluster simulated at comparable resolution, and discuss the relative abundance and survival probabilities of substructure in both simulations. In § 4 we estimate the dark matter self-annihilation γ-rays signal from substructure at $z = 75$ and $z = 0$. Finally, we summarize our conclusions in § 5. Details about finding early CDM substructures both with SKID and a new phase-space friends-of-friends (6DFOF) algorithm are given in the Appendix.

2. N-BODY SIMULATIONS

The results of this paper are based on a comparison between two dark matter simulations on vastly different scales. One simulation ("SUSY") resolves DM substructure all the way down to the free-streaming scale for a generic supersymmetric particle of mass $m_X = 100$ GeV, and is designed to model the formation of the smallest and earliest dark microhalos in the universe. The other simulation ("B9") models the formation of a 5.9×10^{14} $M_\odot$ cluster at the present epoch, and was previously discussed in Diemand, Moore, & Stadel (2004).

Both simulations were performed with PKDGRAV (Stadel 2001; Wadsley et al. 2004) and employed the multiple mass particle grid initial conditions as described in Diemand et al. (2004). The SUSY run has a comoving box size of 3 kpc and was initialized at $z = 456$ using the GRAFICS package (Bertschinger 2001) with a DM power spectrum $P(k)$ for a 100 GeV neutralino (kinetic decoupling occurs at $T_d = 28$ MeV) given in Green et al. (2004)[1]. This power spectrum is close to $P(k) \sim k^{-3}$ and exhibits a free streaming cutoff at $k = 1.65$ (comoving pc)$^{-1}$, corresponding to a mass scale of $1.1 \times 10^{-6}\,M_\odot$. The initial coupling between DM and radiation produces acoustic oscillations that leads to a slightly higher cutoff mass of $4.5 \times 10^{-6}\,M_\odot$ (see eq. 26 in Loeb & Zaldarriaga 2005), but we have neglected this correction in the present work.

TABLE 1
Simulation parameters

z_i	z_f	ϵ (comoving units)	$N_{\rm hires}$	$m_{\rm p,hires}$ ($M_\odot$)
455.8	75.1	0.00216 pc	6.4×10^7	0.98×10^{-9}
40.3	0.0	4.8 kpc	2.8×10^7	5.2×10^7

Note. — Initial and final redshifts z_i and z_f, (spline) softening length ϵ, and number $N_{\rm hires}$ and masses $m_{\rm p,hires}$ of high resolution particles, for the SUSY (*top*) and B9 (*bottom*) runs.

The SUSY simulation is centered on a rare high-σ peak, which is covered by a 120 comoving pc high-resolution region consisting of 64 million DM particles. This results in a mass per particle of $9.8 \times 10^{-10}\,M_\odot$, which ensures that even objects at the free-streaming limit are resolved with ~ 1000 particles. At $z = 75$ the most massive halo in the box has a virial mass[2] of $M_{\rm halo} = 0.014\,M_\odot$, which corresponds to a 3.5-σ fluctuation. We have adopted the standard concordance ΛCDM cosmology with parameters $\Omega_M = 0.268$, $\Omega_\Lambda = 0.732$, $H_0 = 71\,{\rm km\,s^{-1}\,Mpc^{-1}}$, $n = 1$, and a power spectrum normalized to $\sigma_8 \equiv \sigma(z = 0, r = 8\,h^{-1}\,{\rm Mpc}) = 0.9$ in the SUSY and 0.7 in the B9 run. The parameters of both simulations are summarized in Table 1.

3. HALO SUBSTRUCTURE

The k^{-3} dependence of the power spectrum near the SUSY cutoff translates into a $\sigma(M)$ (the linear theory rms density fluctuations extrapolated to the present-day in a sphere containing a a mass M), that is nearly independent of mass. This implies that structures are simultaneously collapsing over a wide range of masses and has important consequences for the nature of DM (sub-) structure near the SUSY cutoff, as we show below.

3.1. *Structure formation on SUSY scales*

In linear theory the collapse time of a typical spherical top-hat overdensity of mass M is given by $\sigma(M)D(a) = \delta_c$, where $D(a)$ is the growth factor and δ_c is the critical overdensity for collapse. Assuming a flat universe with $\Omega_M = 1$ at these early epochs, a typical $10^{-6}\,M_\odot$ microhalo will form at $z = 30$, whereas a much more massive $0.01\,M_\odot$ parent will collapse at $z = 23$, i.e. structure formation on very different mass scales happens almost simultaneously. By contrast, $\sigma(M)$ is significantly steeper on galaxy and cluster scales, which leads to a orderly hierarchical buildup of cosmic structure.

The sequence of nested N-body resimulations of Gao et al. (2005) already showed that large-scale structure at $z \sim 50$ is qualitatively different from that in the low-redshift universe. A comparison between the extremely rapid assembly of our SUSY halo at redshifts $130 < z < 75$ and the canonical hierarchical growth of cluster B9 at late epochs is given in Figure 1. Here we

[1] As in Diemand et al. (2005) we use model "A" of the first preprint version of Green et al. (2004) (astro-ph/0309621v1).

[2] The "virial" mass is defined to enclose a mean density 200 times the mean background density in the high redshift SUSY run. For the $z = 0$ cluster, it is 368 times the mean background density.

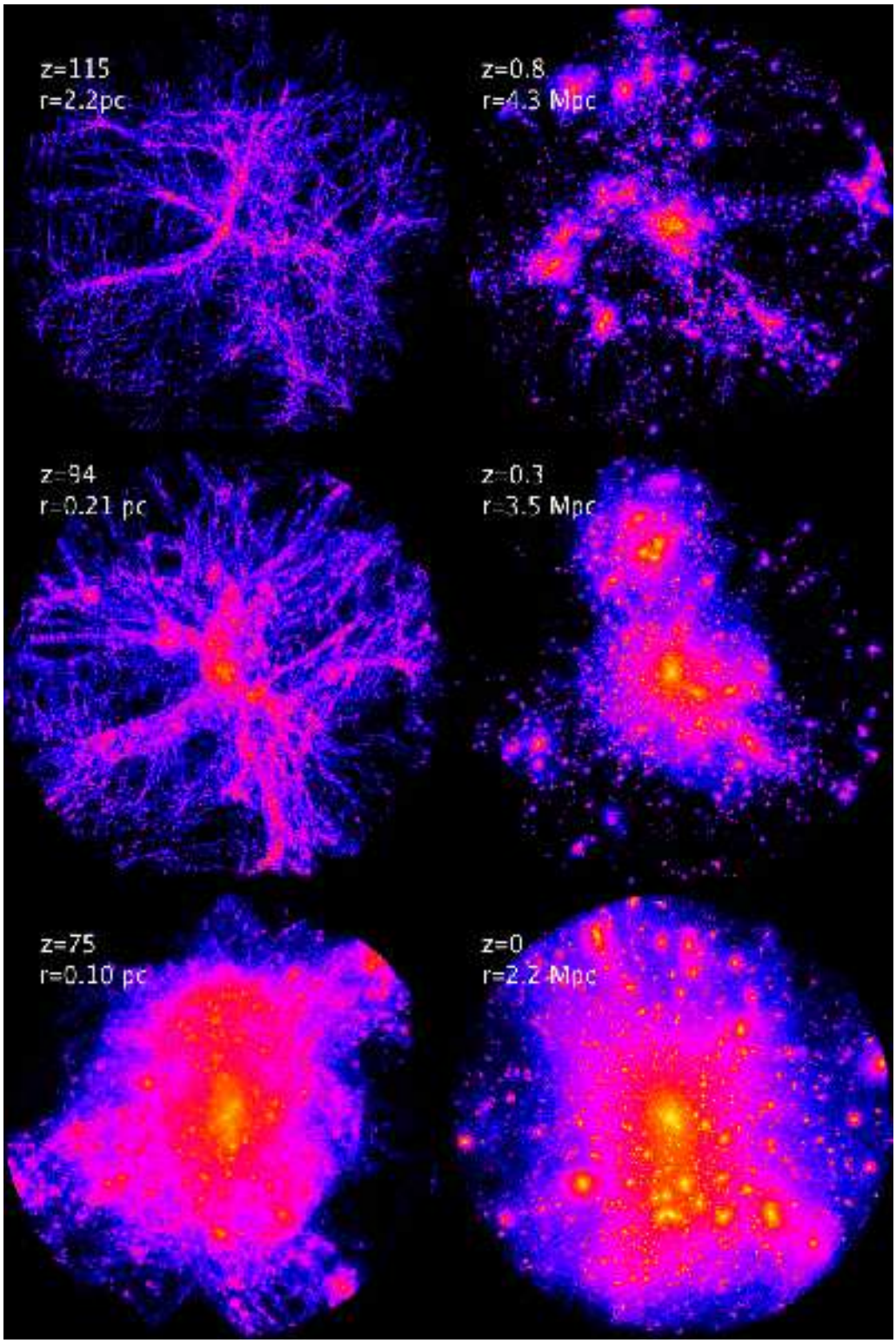

FIG. 1.— Local DM density maps. The left-hand panels illustrate the almost simultaneous structure formation in the SUSY run at different epochs, within a sphere of physical radius r including a mass of 0.014 $M_\odot$ (equal to $M_{\rm halo}$ at $z = 75$). The galaxy cluster halo B9 (*right-hand panels*) forms in the standard hierarchical fashion: the DM distribution is shown within a sphere of radius r including a mass of 5.9×10^{14} $M_\odot$ (equal to $M_{\rm halo}$ at $z = 0$). The SUSY and cluster halos have concentration parameter [defined as $c = 2.15(r_{\rm vir}/r_{\rm v_c,max})$, which is equivalent to $c = r_{\rm vir}/r_s$ for a Navarro-Frenk-White (1997, hereafter NFW) profile] $c = 3.7$ and $c = 3.5$, respectively. In each image the logarithmic color scale ranges from 10 to $10^6 \rho_{\rm crit}(z)$.

show maps of the DM distribution at different epochs within a sphere enclosing the final virial mass of the

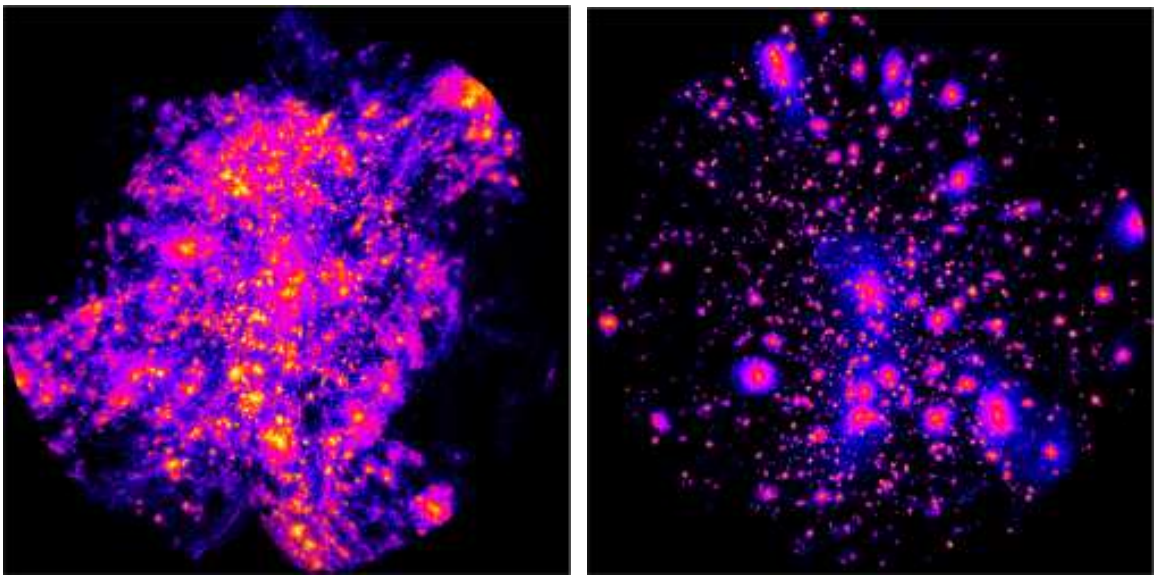

FIG. 2.— Phase-space density map for the $z = 75$ SUSY halo (*left*) and the $z = 0$ galaxy cluster (*right*). Local phase-space densities are estimated using the SMOOTH program (available at www-hpcc.astro.washington.edu/tools/smooth.html) over 32 nearest neighbors. Note the different color scales: relative to the average virial phase-space density ($\bar{\rho}/\bar{\sigma}^3_{\rm 1D}$), the logarithmic color scale ranges from 10 to 10^5 in the SUSY halo and from 10 to 10^7 in the cluster halo.

parent halo, using identical (logarithmic) color scales for direct comparison. The relative sizes of the most massive progenitors are obviously much smaller for the SUSY host than for the cluster. The virial mass of the SUSY halo grows by a much larger factor than B9 during the comparable fractional increase in scale factor shown here. Another consequence of nearly simultaneous structure formation is that filaments are very large relative to the size of the biggest virialised systems in the same region (Gao et al. 2005).

The difference in formation histories discussed above should be reflected in the density contrast between substructure and the host, since the average density at virialization is proportional to the mean density of the universe at the time of collapse. The density contrast scales approximately as the inverse cube of the scale factor at collapse, $(a_{\rm halo}/a_{\rm subh})^3$. For early microhalos of masses $10^{-6}\,{\rm M}_\odot$ and $10^{-2}\,{\rm M}_\odot$ this ratio is only 2.5, much smaller than the typical contrast ~ 20 of galaxy-scale substructure in a cluster host. The expectation is then that substructure in B9 will have significantly higher contrast than in the SUSY halo[3]. Visual inspection of Figure 1 clearly reveals this effect.

Both the SUSY run at $z = 115$ and the B9 run at $z = 0.8$ correspond to epochs when the linear growth factor is about 0.66 of the final value at $z = 75$ and $z = 0$, respectively. At $z = 115$ we find 1931 virialized microhalos, less than the 2906 galaxy-size halos and subhalos in the cluster forming region at $z = 0.8$. The abundance of bound halos in the SUSY run becomes similar to B9 only around $z \approx 100$. The fractional size of the most massive progenitor is also smaller in the SUSY run: at $z = 115$ this has a mass of $0.01\,M_{\rm halo}(z = 75)$, while the largest cluster progenitor at $z = 0.8$ has already a mass of $0.25\,M_{\rm halo}(z = 0)$. It takes until $z \approx 90$ before the SUSY main progenitor has also grown to a virial mass of about one quarter of the final system. This illustrates the compression of host- and subhalo formation times resulting from the flatness of $\sigma(M)$ on extremely small scales.

Subhalos have smaller internal velocity dispersions than the hot uniform density background. Therefore subhalos stand out much more clearly in phase-space density $\rho/\sigma^3_{\rm 1D}$ than in real space density, as shown in Figure 2. The phase-space map reveals that the SUSY halo indeed has rich substructure at $z = 75$, comparable in abundance to the $z = 0$ B9 cluster. Yet as in physical density, the phase-space density contrast is lower in the SUSY run compared to the B9 halo. Note the different color scales in Figure 2: the scale spans six decades in the B9 image, but only four decades in the SUSY image.

3.2. *Substructure mass function*

We have constructed substructure catalogs for the SUSY and B9 hosts at various stages in their formation. We employ two different algorithms to identify subhalos: a) SKID (Stadel 2001), which gives reliable subhalo masses by iteratively removing unbound particles, but is computationally expensive; and b) a new phase-space friends-of-friends method (6DFOF), which only produces halo centers and maximum circular velocities, but is significantly faster than SKID and is designed to take advantage of the higher substructure contrast in phase-space. Both techniques are described in more detail in Appendix A. Because of the reduced contrast at high redshift, the SUSY sub-microhalo catalogs depend strongly on our choice of identification method and parameters, much more so than in a $z = 0$ cluster like B9. Nevertheless we find reasonable agreement between the

[3] This simple argument is strictly valid only for typical 1σ fluctuations of the density field. Subhalos are likely to have a slightly larger contrast, since they form from rarer fluctuations that are superposed on their parent halo density peak.

two methods when SKID is run with a linking length of 0.0216 comoving pc and a smoothing scale of 1024 nearest neighbors (cf. Appendix A).

We define a dimensionless subhalo mass, $M_{\rm subh}/M_{\rm halo}$, and plot in Figure 3 the abundance of SUSY sub-microhalos at $z = 86$ and $z = 75$ against this normalized mass. The normalized mass function lies close to and within the scatter of the average normalized subhalo mass function found in galaxy clusters at the present epoch, a self-similarity that has been previously found to hold over a wide range of mass scales and redshifts, from present-day clusters to dwarf galaxy halos at $z = 4$ (Moore et al. 2001), and even for 10^5 $M_\odot$ host minihalos at $z = 49$ (Gao et al. 2005). Our simulations extend this range down to 10^{-2} $M_\odot$ SUSY hosts at $z \gtrsim 75$: the substructure populations of young, low-concentration halos are approximate scaled copies of each other, independent of parent mass. Note that the same self-similarity also appears in the normalized distribution of subhalo maximum circular velocities (see Figure 4).

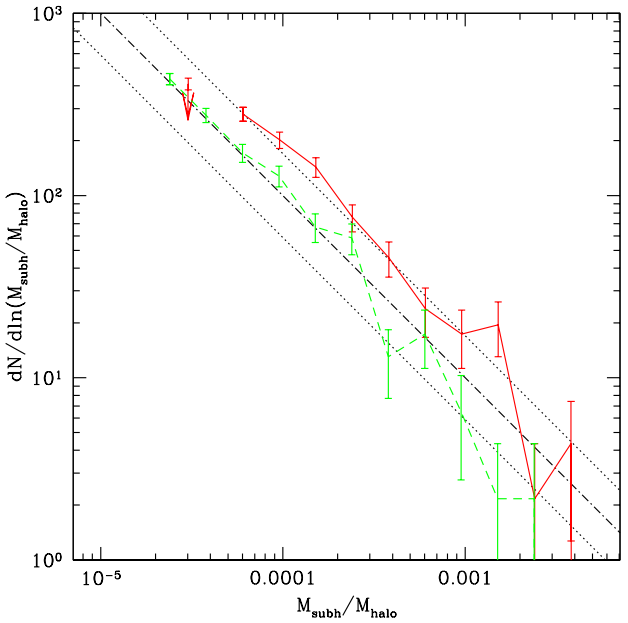

FIG. 3.— Differential SUSY sub-microhalo abundance as a function of scaled sub-microhalo mass, $M_{\rm subh}/M_{\rm halo}$, at $z = 86$ (*solid*) and at $z = 75$ (*dashed*). Halo masses were determined by SKID using $s = 1024$. The dash-dotted line corresponds to $dN/d\ln(M_{\rm subh}/M_{\rm halo}) = 0.01(M_{\rm subh}/M_{\rm halo})^{-1}$, which is a good approximation to the $z = 0$ galaxy cluster relation (Diemand et al. 2004). The dotted lines show the scatter (≈ 0.23 dex) around this relation. The first bin begins at 256 bound particles. Bars show the Poisson errors. The arrow shows the upper limit for the abundance of sub-M_c clumps (128 to 202 bound particles) at $z = 86$ estimated by using SKID with $s = 64$ (see Appendix for details).

In Figure 5 we present the non-normalized circular velocity function for our set of SUSY sub-microhalos. The circular velocity distribution for subhalos of $20 - 300$ km s^{-1} in hosts of mass $10^{11} - 10^{14}$ $M_\odot$ at redshifts from zero to two is fitted by (Reed et al. 2005)

$$\frac{dn}{dv_{\rm c,max}} = 1.5 \times 10^8 v_{\rm c,max}^{-4.5} ({\rm h^3 Mpc^{-3} km^{-1} s}) \ , \qquad (1)$$

has little or no trend with host mass or redshift. The figure shows that our SUSY sub-microhalo velocity function at $z = 86$ lies right on the extrapolation (over four orders of magnitude) of equation (1). The sub-microhalo abundance appears to decrease with cosmic time until the last analyzed snapshot at $z = 75$, where it is still within the scatter around the universal function of Reed et al. (2005). Unfortunately we cannot quantify the substructure abundance at lower redshifts since the parent halo is growing very quickly and starts accreting material from the lower resolution regions, in the form of heavier particles. Note that the evolution in the subhalo mass or circular velocity functions should not be used to constrain the survival probability of substructure, since the mass of the host (and hence the volume probed) increases significantly with time.

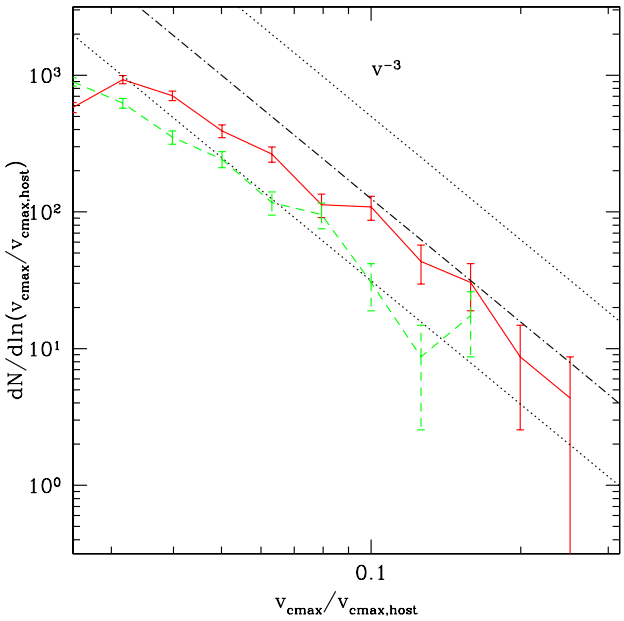

FIG. 4.— Differential SUSY sub-microhalo abundance as a function of scaled maximum circular velocity, $v_{\rm c,max}/v_{\rm c,max,host}$, at $z = 86$ (*solid*) and $z = 75$ (*dashed*). Halos were identified with a phase-space friend-of-friend finder (6DFOF). The dash-dotted line is the universal normalized circular velocity function of substructure in hosts of 1011 to 10^{14} $M_\odot$ found by Reed et al. (2005) at $0 < z < 2$, $dN/d(v_{\rm c,max}/v_{\rm c,max,host}) = (1/8)(v_{\rm c,max}/v_{\rm c,max,host})^{-4}$. The reported halo-to-halo variance in the scatter around the universal circular velocity distribution is a factor of 2 to 4, the dotted lines illustrate deviations by factors of four.

3.3. *Formation of halos below the cutoff scale*

The SUSY-CDM scenario adopted here has an exponential cutoff in the power spectrum $P(k)$ at a scale corresponding to a mass of $M_c = 10^{-6}$ $M_\odot$. Below this mass the formation of structures is suppressed relative to a CDM scenario without such a cutoff (Diemand et al. 2005). But the suppression is not total: some halos and subhalos with masses well below M_c do actually form. The formation, abundance and properties of halos below a cutoff scale has been studied in detail in the context of warm dark matter (WDM) models, both for field halos (e.g. Bode et al. 2001; Knebe et al. 2003; Yoshida et al. 2003) and subhalos (e.g. Colín et al. 2000; Yoshida et al. 2003). A quantitative comparison with these results lies beyond the scope of this work. In this section we illus-

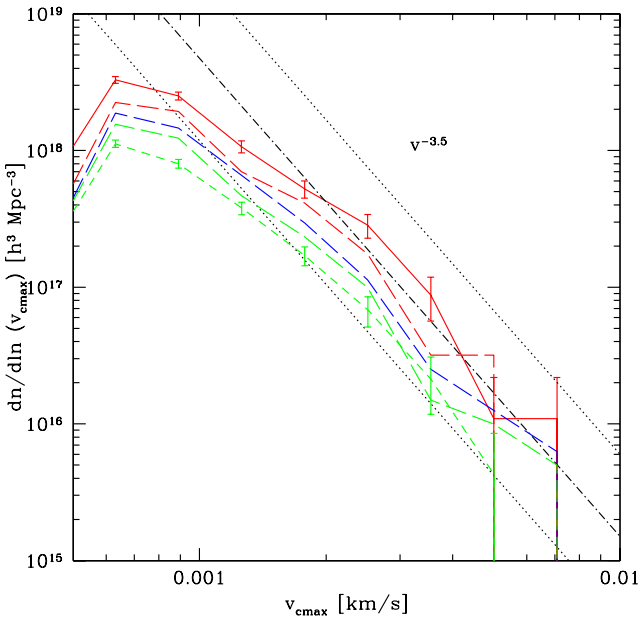

FIG. 5.— SUSY sub-microhalo circular velocity function at $z = 86$ (*solid curve*), $z = 83, z = 80, z = 78$ (*long-dashed curves*, from top to bottom), and $z = 75$ (*short-dashed curve*). Volume units are comoving. The solid straight line is the universal subhalo velocity function of Reed et al. (2005), extrapolated from $20 - 300$ km s^{-1} down to scales of ms^{-1}. The dotted lines illustrate deviations by factors of four.

trate one formation path of sub-M_c halos and place an upper limit on their abundances in order to ensure that DM clumps below M_c do not provide a significant contribution to the DM annihilation signal.

The perturbed cubic grid initial conditions used here have a characteristic length scale and preferred directions, which is not the case for unordered "glass" initial conditions (White 1993). Götz & Sommer-Larsen (2003) suggested that grid initial conditions lead to artificial fragmentation of WDM filaments and that glass initial conditions should be used instead to overcome this problem. Even glass WDM simulations show the formation of sub-cutoff objects (Yoshida et al. 2003), however, meaning either that glass initial conditions do not prevent artificial fragmentation or that the formation of sub-cutoff structure is real. Our sub-M_c halos do not form with a preferred separation or along the initial grid axis (see Figs. 1 and 6), which implies that they are not artifacts produced by regular grid noise in the initial conditions.

Figure 6 shows the formation of a clump of mass 0.3×10^{-6} M$_\odot$ at $z = 86$. This halo forms 'top-down' through the fragmentation of a filament, like the smallest WDM halos seen in Knebe et al. (2003). Note that the fragmentation occurs only after the formation of larger halos in the same region, i.e. the sub-M_c clump forms after its larger neighbors and it therefore has a lower peak density and concentration. One can think of the sub-M_c clump as a low amplitude initial overdensity on some scale larger than M_c which fails to grow to a mass above M_c: by the time the low amplitude perturbation goes non-linear its larger and higher amplitude neighbors have already collapsed and are accreting some of the mass which in linear theory would correspond to the smaller, low amplitude peak. The small peak collapses at a later time in a relatively depleted environment and fails to grow above M_c.

Structures above $M_c = 10^{-6}$ M$_\odot$ from almost at the same time (see section 3.1) and those below M_c appear to form even later. This explains the low concentration and density contrast of sub-M_c clumps. Their measured abundance depends strongly on the operational definition of substructure, i.e. on the subhalo finding algorithm used and its parameter values (see Appendix for details). The largest abundance of sub-M_c clumps is found with SKID using a density estimate over 64 particles (see Figure A9). This abundance must be taken with caution, however, since many of the smaller groups identified in this way do not show up as significant peaks in local density or phase-space density maps. We use the $s = 64$ SKID value only as an upper limit to the number sub-M_c clumps. It demonstrates that the subhalo mass function becomes much shallower than $dn/dM_{\rm subh} \propto M_{\rm subh}^{-2}$ below about $0.5\,M_c$ (Figure 3). Together with their late formation times and low concentration this is sufficient to exclude a significant contribution to the DM annihilation signal (see section 4) from clumps below M_c.

3.4. *Survival*

In order to properly quantify the survival probabilities and robustness against tidal stripping of subhalos at high and low redshift we have traced substructure in the entire high resolution region forward in time. We examine three time intervals, each covering a comparable increase in scale factor. Because of the rapid assembly of the SUSY halo we are limited to a relatively small ratio of final to initial scale factor, $a_f/a_i \approx 4/3$, i.e. from $z_i = 115$ to $z_f = 86$ and from $z_i = 101$ to $z_f = 75$ for the SUSY halo, and from $z_i = 0.333$ to the present epoch for the B9 cluster. Subhalos are identified with 6DFOF (see Appendix A) and we consider only halos with more than 320 linked particles at z_i, an order of magnitude larger than our usual choice of 32 linked particles at z_f. This allows us to identify surviving structures that have lost a large fraction of their mass (up to 90 percent) due to tidal effects. A halo at z_i is counted as a survivor if it contributes at least 10 particles to some halo at z_f, unless it has merged with the central core of the z_f parent system. Note that even halos for which we find no remnant may actually have one at higher numerical resolution.

We approximate the Lagrangian region of the particles that will end up within the virial radius of the parent at z_f by a sphere of radius $R_{\mathcal{L},\rm vir}$ centered on the most massive progenitor (MMP) at z_i, and enclosing a mass $M_{\rm halo}(z_f)$. Halos within $R_{\mathcal{L},\rm vir}$ at z_i are likely to end up within $r_{\rm vir}$ at z_f. Table 2 summarizes the survival probabilities of well resolved substructure as a large host system is forming. Considering all halos in the high resolution region (top three rows) we see that early substructure is significantly more likely to be disrupted, with more than 99% of all subhalos surviving from $z_i = 0.333$ down to the present epoch, but only 87% surviving from $z_i = 115$ to $z_f = 86$ and even less (73%) from $z_i = 101$ to $z_f = 75$. Tidal destruction is more efficient closer to the center of the host, and this causes a further reduction in the survival fraction of substructure within two

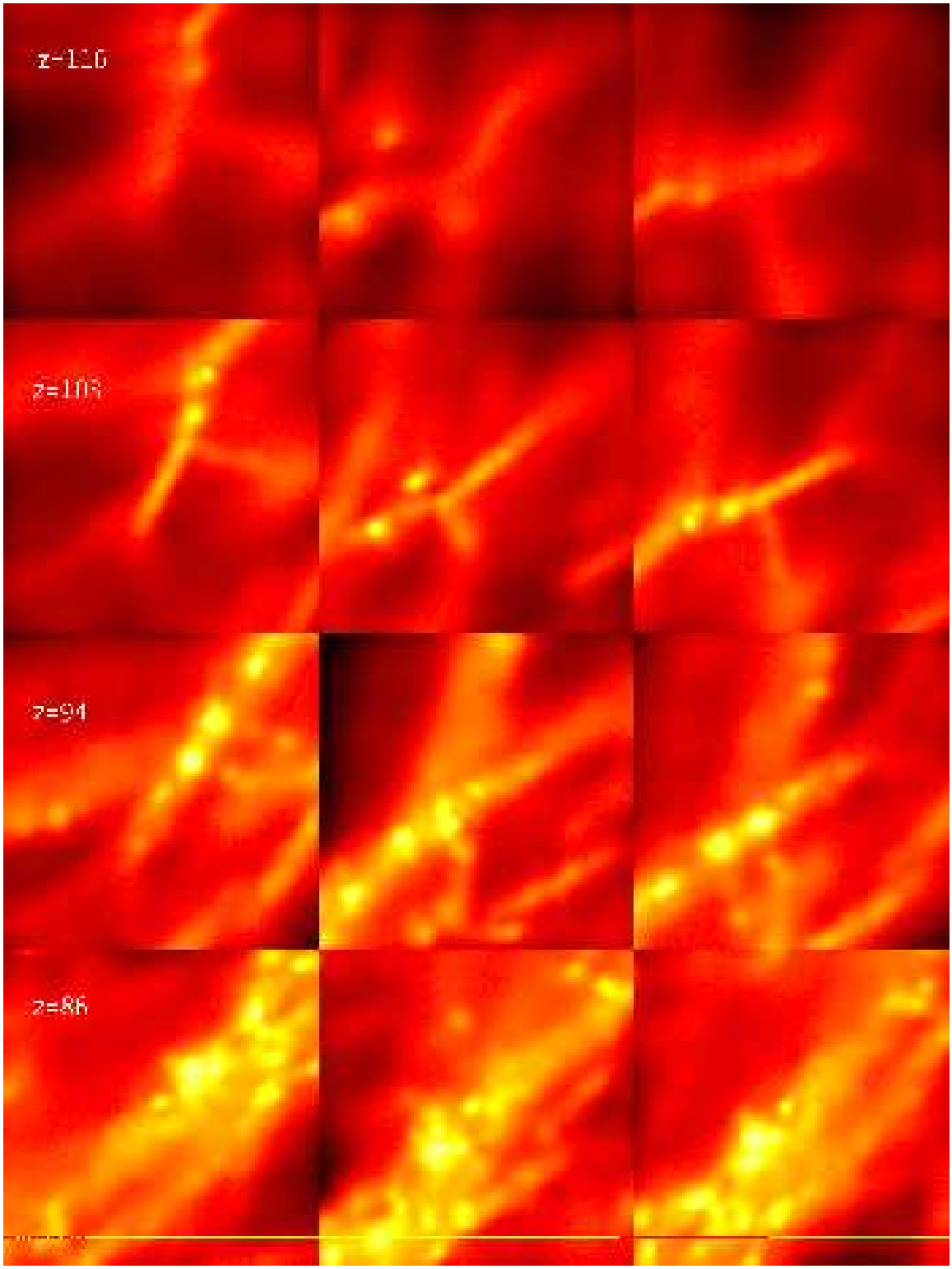

FIG. 6.— Projected DM density maps illustrating the formation of a halo with $M_{\rm halo} = 0.3 \times 10^{-6}$ M$_\odot$, i.e. below the cutoff scale of $M_c = 10^{-6}$ M$_\odot$. Three orthogonal projections of the same cube are shown at each time. The cubes have a size of $L = 2.7$ comoving pc and are centered on those particles which end up in the sub-M_c clump at $z = 86$. The logarithmic color-scale goes from $\rho_{\rm crit}(z)\ L$ to $10^{2.4}\rho_{\rm crit}(z)\ L$ at all times. The whole region is relatively overdense: its mean density increases from $6\rho_{\rm crit}(z)$ at $z = 116$ to $21\rho_{\rm crit}(z)$ at $z = 86$. The three projection directions are aligned with the axes of the initial grid and the initial particle spacing of 0.3 comoving pc is indicated by the ruler in the lower-right panel. Note that these structures do not show a preferred direction, alignement with the axes of the initial grid, or any regular, grid-scale separation which would indicate artificial fragmentation caused by the grid initial conditions.

(middle three rows) or one $R_{\mathcal{L},\rm vir}$ (bottom three rows). In Figure 7 we plot the survival fraction versus distance

TABLE 2
NUMBERS AND FRACTIONS OF SURVIVING STRUCTURES

Region	z_i	z_f	$N_{\rm tot}$	$N_{\rm sur}$	$f_{\rm sur}$	$N_{\rm core}$	$F_{v_{\rm c,max}}$
all	115	86	150	131	0.873	3	1.286
	101	75	227	165	0.727	2	0.954
	0.333	0	774	771	0.996	1	0.956
$< 2R_{\mathcal{L},\rm vir}$	115	86	111	94	0.847	3	1.242
	101	75	206	145	0.704	2	0.944
	0.333	0	497	494	0.994	1	0.925
$< R_{\mathcal{L},\rm vir}$	115	86	75	58	0.773	3	1.033
	101	75	121	75	0.620	2	0.765
	0.333	0	261	258	0.989	1	0.8414

NOTE. — Substructure is identified based on phase-space density (using 6DFOF) at z_i and its survival is checked at z_f. $N_{\rm tot}$ and $N_{\rm sur}$ are the total number and number of surviving halos, and $f_{\rm sur} = N_{\rm sur}/N_{\rm tot}$ denotes the fraction of surviving substructure. $N_{\rm core}$ is the number of halos merging with the core of the z_f halo. $F_{v_{\rm c,max}} = \langle v_{\rm c,max,i}\rangle/\langle v_{\rm c,max,f}\rangle$ denotes the ratio of the initial to final average maximum circular velocity. The first group of three rows is for the entire high resolution regions, the second and third groups are for substructures initially within two and one $R_{\mathcal{L},\rm vir}$, respectively, where $R_{\mathcal{L},\rm vir}$ is the radius encompassing $M_{\rm halo}(z_f)$ at z_i. See text for details on the 6DFOF phase-space halo finder and on how survival is determined.

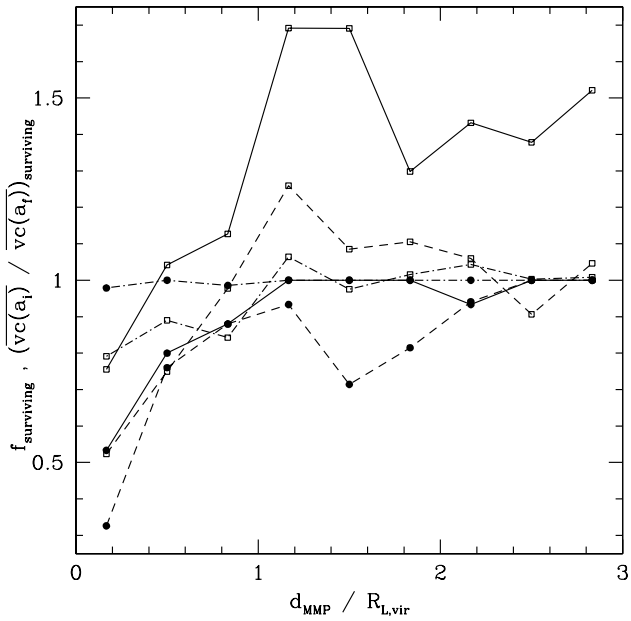

FIG. 7.— Fraction of surviving structures (*solid circles*) and ratios of initial to final average circular velocity $v_{\rm c,max}$ of surviving substructure (*open squares*) versus initial separation from the most massive progenitor in units of $R_{\mathcal{L},\rm vir}$. Halos were traced from $z_i = 115$ down to $z_f = 86$ (*solid lines*), from $z_i = 101$ to $z_f = 75$ (*dashed*), and from $z_i = 0.333$ down to the present epoch (*dash-dotted*).

to the MMP in units of $R_{\mathcal{L},\rm vir}$, $d_{\rm MMP}$, for the three time epochs analyzed. This drops rapidly for $d_{\rm MMP} \lesssim R_{\mathcal{L},\rm vir}$ in the case of SUSY sub-microhalos, below 50% (30%) for the epoch ending at $z_f = 86$ ($z_f = 75$).

The subhalos that do survive experience significant mass loss due to tidal stripping. We quantify this mass loss by calculating the ratio of the average of $v_{\rm c,max}$ of all halos at the beginning to that at the end of each epoch, $F_{v_{\rm c,max}} \equiv \langle v_{\rm c,max,i}\rangle/\langle v_{\rm c,max,f}\rangle$ (Figure 7). For halos beyond $R_{\mathcal{L},\rm vir}$ $v_{\rm c,max}$ grows with time in the SUSY simulation, whereas for B9 the ratio remains about constant. The increase in average $v_{\rm c,max}$ is especially strong in the redshift interval $115 - 86$, $F_{v_{\rm c,max}} \approx 1.5$, and this again illustrates the rapid and late (in terms of a_f/a_i) formation and growth of these structures. SUSY sub-microhalos within $R_{\mathcal{L},\rm vir}$ suffer more mass loss than those beyond $R_{\mathcal{L},\rm vir}$, $F_{v_{\rm c,max}}(< R_{\mathcal{L},\rm vir}) = 0.68 F_{v_{\rm c,max}}(> R_{\mathcal{L},\rm vir})$. For the cluster substructure the difference between outer and inner regions is less pronounced, indicating that it is more resistant against tidal stripping. This robustness translates into a higher survival probability, as shown above.

4. DARK MATTER ANNIHILATION SIGNAL

The differences in substructure contrast described in the previous sections have ramifications for the expected γ-ray signal from DM self-annihilation. Indirect detection experiments are hoping to detect both the cosmological extragalactic background as well as the local signal from the Milky Way's center and from DM substructure in its halo. Since the annihilation rate is proportional to $\rho^2_{\rm DM}$, the predicted flux depends sensitively on the clumpiness of the DM distribution. Small-scale substructure is expected to significantly increase the signal from individual halos (Calcaneo-Roldan & Moore 2000; Stoehr et al. 2003; Colafrancesco et al. 2005), as well as the the diffuse extragalactic background (Ullio et al. 2002; Taylor & Silk 2002; Ando & Komatsu 2006). Annihilation luminosity estimates based on DM densities measured in collisionless N-body simulations of a Milky Way-scale halo suggest that substructure may boost the signal by only a small factor, $\sim 70\%$, compared to a smooth spherical NFW halo (Stoehr et al. 2003, hereafter S03). In this work we follow S03's analysis and compare the contribution of substructure in the SUSY host at $z = 75$ and the B9 galaxy cluster at $z = 0$.

The annihilation luminosity is proportional to the ratio of the velocity weighted self-annihilation cross section and the mass of the DM particle, $\langle\sigma v\rangle/m_X$. Following S03, we disregard this (highly uncertain) particle physics term and concentrate instead on the astrophysical component, defining the annihilation signal of the $i^{\rm th}$ halo to be

$$S_i = \int_{V_i} \rho^2_{\rm DM} dV_i = \sum_{j\epsilon\{P_i\}} \rho_j m_j, \qquad (2)$$

where ρ_j and m_j are the density and mass of the $j^{\rm th}$ particle, and $\{P_i\}$ is the set of all particles belonging to halo i. Whereas S03 estimated the ρ_j with the parameter-free Voronoi tessellation technique, we use the SPH-kernel estimated densities from SMOOTH over 64 nearest neighbors.

Like S03 we find that the component from the spherical-average density profile contributes only a fraction of the total signal, 49% in the SUSY halo and only 35% in the B9 halo. The contribution to the signal from all resolved bound subhalos is 39% in B9 and only 10% in the SUSY host. The remaining difference is due to both unbound streams and departures from spherical symmetry[4]. The absolute contribution of the resolved substruc-

[4] These estimates depend only weakly on the smoothing scale

ture component depends on numerical resolution, since higher resolution simulations would be able to resolve higher densities in the subhalo centers (Kazantzidis et al. 2004). The bound substructure contribution to the total signal could be larger and the values given here should be taken as lower limits. Both the SUSY and B9 halos, however, have approximately the same number of particles within their virial radii, allowing us to directly compare the contribution from resolved substructure between the two. We conclude that it is indeed the lower density contrast in the early SUSY host that leads to a significantly smaller contribution from bound sub-microhalos to the total annihilation signal.

used for the SPH density estimates: using 1024 instead of 64 nearest neighbors gives relative contributions of spherical smooth signal, bound substructure, and remaining density fluctuations of $(57\%, 9\%, 34\%)$ instead of $(49\%, 10\%, 40\%)$ for the $z = 75$ SUSY halo.

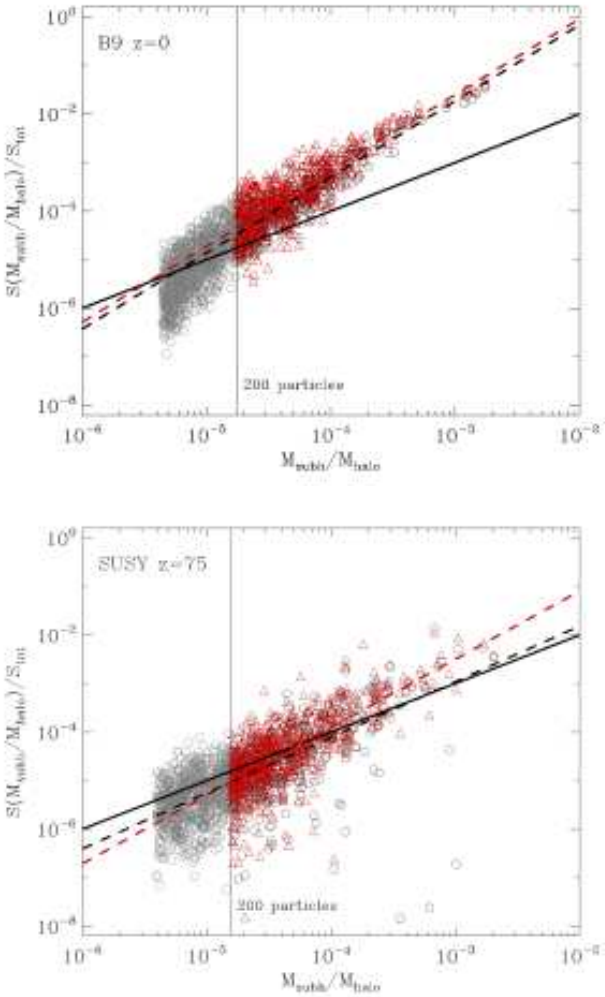

FIG. 8.— The ratio of the annihilation signal of individual subhalos to the total signal from all dark matter particles in the host halo versus the subhalo mass ratio $M_{\rm subh}/M_{\rm halo}$. Circles denote the signal calculated directly from the subhalo particle densities, triangles are used for an estimate of the signal assuming an NFW profile and a concentration $c \approx 2r_{\rm vir}/r_{\rm v_{c,max}}$. The top panel shows the B9 halo at $z = 0$, the bottom one the SUSY halo at $z = 75$. Subhalos with the same signal-to-mass ratio as the host would lie on the thick solid line. The dashed lines show the best-fit linear relation between subhalo signal and normalized mass (*lower line:* direct calculation, *upper line:* NFW estimate). Halos to the right of the thin vertical line have more than 200 particles.

In Figure 8 we present the mass dependence of the annihilation signal for individual subhalos. To ease a direct comparison we normalize the subhalo mass by the total halo mass and the subhalo signal by the total signal from all halo DM particles. Since the signal strength may depend sensitively on the internal density structure of the subhalo, we only include halos with more than 200 particles in our analysis. If substructure had the same signal-to-mass ratio S/M as their host they would lie on the thick solid line in the figure. We find instead that the B9 subhalos tend to have a larger S/M (i.e. they lie above the solid line, in qualitative agreement with S03), but that the majority of the SUSY sub-microhalos have lower S/M than their host. Furthermore we find that S/M is not independent of mass: in both our simulations less massive substructures have a lower S/M than

more massive ones. For B9 we find $S/M \propto M_{\rm subh}^{0.5}$, while for SUSY $S/M \propto M_{\rm subh}^{0.4}$. Given a substructure abundance of $dN/dM_{\rm subh} \propto M_{\rm subh}^{-\alpha}$ with $\alpha \lesssim 2$ (see Section 3.2), this suggests that the total signal may be dominated by the highest mass subhalos. One has to keep in mind, however, that the peak densities in an N-body halo are always limited by numerical resolution. The local densities are too low both in the center of the host system (Diemand et al. 2004) and even more so in the inner regions of subhalos (Kazantzidis et al. 2004). It is thus likely that estimates of the total annihilation signal based directly on densities measured in N-body halos underestimate the importance of the substructure contribution. Analytic calculations (Calcaneo-Roldan & Moore 2000) tend to find larger substructure boost factors and a signal that is dominated by small subhalos (Colafrancesco et al. 2005).

We have attempted to correct for the artificial heating of the densest, inner regions by recalculating the annihilation signal for every subhalo assuming an NFW profile with a concentration given by $c \approx 2.16 r_{\rm vir}/r_{\rm v_{c,max}}$. In this case the normalized annihilation signal is equal to

$$\tilde{S}/S_{\rm tot} \approx 1.22 \left(\frac{v_{\rm c,max}^4}{G^2 r_{\rm v_{c,max}}} \right) / S_{\rm tot}, \qquad (3)$$

where G is the gravitational constant, and $v_{\rm c,max}$ and $r_{\rm v_{c,max}}$ are determined using SKID with spherical binning of the bound subhalo particles. Expressing $\tilde{S}_i$ in terms of $v_{\rm c,max}$ and $r_{\rm v_{c,max}}$ reduces the dependence of the estimate on the strongly resolution dependent inner density profile. These corrected subhalo signals are plotted as triangles in Figure 8. As expected the NFW estimate enhances the signals, and the correction is about 30% in both the SUSY and the B9 halo. With this boost the relative contributions of spherical smooth signal, bound substructure, and remaining density fluctuations are $(47\%, 14\%, 39\%)$ for the SUSY and $(30\%, 48\%, 22\%)$ for the B9 halo. Note that the substructure signal in the B9 run is still significantly larger than in the SUSY run. The mass dependence of S/M appears to be preserved, but we caution that even our NFW estimates are not bias free: the finite resolution in our simulations may well lead to an underestimate of $v_{\rm c,max}$ (cf. Kazantzidis et al. 2004), especially for low-mass subhalos.

Our results suggest that in a real sub-solar mass SUSY halos the signal from subhalos and other density fluctuations is at least as big as the signal from the spherically-averaged component. Estimates of the cosmological, extragalactic γ-ray background (Ullio et al. 2002; Taylor & Silk 2002; Ando & Komatsu 2006) should be revised to take into account both microhalos in the field (Diemand et al. 2005) and sub-microhalos within larger (sub)-solar mass systems like the one studied in this work. We plan to address remaining open questions (i.e. the total substructure boost factor and what subhalo mass scale dominates the signal) in future work using higher resolution simulations, extensive convergence tests, and comparisons with various analytical estimates.

5. CONCLUSIONS

We have simulated the formation of a 0.014 $M_\odot$ halo at $z = 75$ in a scenario where CDM consists of 100 GeV supersymmetric particles. Our main results are:

- Early SUSY-CDM structures form almost simultaneously over a wide range of mass scales. Halo masses grow very rapidly, and filaments are very extended compared to the size of the largest halos.
- The contrast between substructure and background is lower in early SUSY halos than in galaxy cluster hosts, both in density and in phase-space density.
- At $z = 0$ a simple, fast phase-space friends-of-friends subhalo finder (6DFOF) gives robust results. Velocity functions and subhalos number density profiles are identical to those obtained with SKID. Unfortunately on SUSY scales both methods have problems due to the reduced contrast. Results from both methods depend quite strongly on the input parameters, but can be brought into agreement with a suitable choice of parameters.
- In relative units both the sub-microhalo mass and circular velocity functions of the 0.014 $M_\odot$ SUSY host are in the range found for $z = 0$ galaxy clusters.
- In absolute units both the circular velocity functions of the 0.014 $M_\odot$ host halo lie within the scatter of the universal subhalo circular velocity function found by Reed et al. (2005) in low redshift dwarf, galaxy, and cluster halos.
- As the universe expands by a factor of 1.3, about 20 to 40 percent of well-resolved early substructure is destroyed, compared to only about 1 percent in the low-redshift cluster. The reductions in the peak circular velocities among the survivors are also larger for the early micro-subhalos.
- The contribution to the DM annihilation signal from the bound sub-microhalos resolved in our simulations is about four times smaller than the signal from the spherically-averaged component in the SUSY host. In a cluster simulated at similar numerical resolution (B9), the bound substructure contribution exceeds the spherically-symmetric part. Due to numerical limitations these are lower limits. The reduced contrast in early-forming sub-microhalos results in a lower substructure boost factor compared to galaxy or cluster halos.

ACKNOWLEDGMENTS

We would like to thank the referee for helpful comments. It is a pleasure to thank Joachim Stadel for making PKDGRAV available to us and for his help with the implementation of the 6DFOF group-finder. We thank Tom Abel, Andreas Faltenbacher, Ben Moore, Joel Primack and Simon White for useful and motivating discussions. J.D. especially thanks Paul Schechter and Ed Bertschinger for discussions and suggestions during the MKI dark matter substructure workshop at MIT. Support for this work was provided by NSF grant AST02-05738 and NASA grant NNG04GK85G (P.M.), and by the Swiss National Science Foundation (J.D.). Simulation B9 was run on the zBox supercomputer at the University of Zurich, while the SUSY run was performed on NASA's Project Columbia supercomputer system.

APPENDIX

IDENTIFICATION OF EARLY SUSY-CDM MICRO-SUBHALOS

The simultaneous nature of structure formation near the SUSY cutoff scale at early times leads to substructure with a reduced contrast both in real and phase-space density. Conventional subhalo finders use positional information in the group finding stage and velocities only after the fact to decide which particles are gravitationally bound to a subhalo. In this appendix we discuss how a conventional subhalo finder (SKID) performs in these challenging low contrast systems and present a simple and fast new method of finding (sub-)structures in phase-space.

SKID: self bound over-densities

SKID (publicly available at: www-hpcc.astro.washington.edu/tools/skid.html) is described in detail in Stadel (2001). In a dark matter only simulation the group-finding algorithm goes through the following steps. First, the local densities are calculated using an compact SPH kernel whose scale is adjusted for each particle to includes a fixed number 's' of nearest neighbors (the same method is used in the program SMOOTH available at www-hpcc.astro.washington.edu/tools/smooth.html). Second, particles are moved along the density gradients until they move less than a user specified length ϵ, i.e. they are trapped in a local potential well of scale ϵ. When all particles satisfy this criterion, they are linked together using a linking length equal to ϵ. Finally the gravitationally unbound particles are removed iteratively (one by one) from all the groups.

SKID results depend on two parameters: the linking length ϵ and the number of nearest neighbors s. A small ϵ tends to underestimate the mass of larger subhalos while a large ϵ links nearby subhalos together. In current high resolution $z = 0$ CDM clusters (roughly ten million particles within the virial radius) setting $\epsilon = 0.004\, r_{\rm vir}$ successfully identifies most resolved structures. Combining subhalo catalogs derived with a range of values for ϵ results in small corrections at the low mass and high mass end of the subhalo mass function (Ghigna et al. 2000; Diemand et al. 2004). For the $z = 86$ SUSY halo we find a similar weak ϵ-dependence of the SKID results.

The number of nearest neighbors s is usually set to $s = 64$ and in a $z = 0$ CDM cluster the SKID subhalo mass and velocity functions are practically independent of s, with the exception that some subhalos with less than about $0.25s$ bound particles are lost when a larger smoothing scale is used (see Figures A9 and A11). Unfortunately SKID's results are much more parameter dependent for the SUSY halo: the right panel of Figure A9 shows that the SUSY subhalo mass function depends on s over the entire subhalo mass range. Many of the small subhalos found with $s = 64$ and $s = 256$ appear spurious, i.e. visual inspection fails to identify a clear corresponding peak in the mass (or phase space) density projections. Only at the high mass end there is hint of convergence when using $s > 1000$. Tests in the $z = 0$ cluster suggest that using large s leads to an underestimates of the subhalo abundance below about $0.25s$ bound particles. We compromise and use $s = 1024$ throughout the paper, but caution the reader that the resulting group catalogs are probably incomplete below about 256 bound particles.

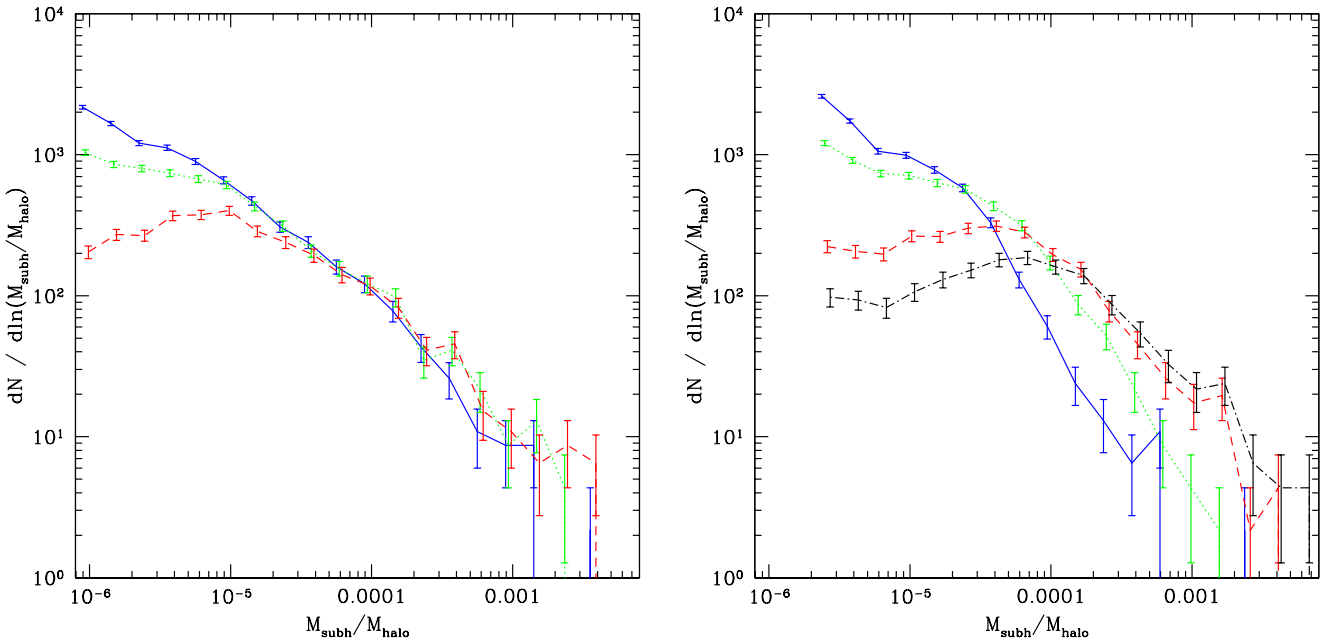

FIG. A9.— SKID subhalo mass functions for the $z = 0$ galaxy cluster (*left*) and the $z = 86$ SUSY CDM halo (*right*) using different numbers of neighbors s for the SPH density calculation. Plotted are $s = 64$ (*solid*), 256 (*dotted*), 1024 (*dashed*), and 2048 (*dash-dotted*, SUSY halo only). The first bin always begins at 10 bound particles. Bars show the Poisson errors. For the massive halo, the mass functions are independent of s above about $0.25s$. Due to the smaller density contrast the entire mass function depends on s for the microhalo.

Finding structures in phase-space: 6DFOF

Subhalos have smaller internal velocity dispersions σ than the hot uniform density background. Figure 2 show maps of ρ/σ^3 (both ρ and σ are calculated using an SPH kernel over 32 nearest neighbors), which is a simple and fast way to estimate the local phase-space density. The phase-space density contrast is much larger than the real-space density contrast. Even small subhalos, which due to limited numerical resolution don't reach peak mass densities as high as their host halo, stand out more clearly in phase-space density because internal velocity dispersions are smaller for less massive halos. In order to take advantage of the increased contrast in phase-space we have developed a new, simple, and fast (sub-)halo finder.

The algorithm is based on the friends-of-friends algorithm (FOF) (Davis & Djorgovski 1985), in which particles are linked together if they are separated by less than some linking length $b \times dx$, where $b < 1.0$ and dx is the mean particle separation. We simply extend the standard FOF algorithm to include also a proximity condition in velocity space. Two particles are linked if

$$(\vec{x_1} - \vec{x_2})^2/(b \times dx)^2 + (\vec{v_1} - \vec{v_2})^2/b_v^2 < 1 \quad , \tag{A1}$$

where b is the standard FOF linking length in units of the mean particle separation dx and b_v^2 is the velocity space linking length. For $b_v^2 \to \infty$ one recovers the usual real-space FOF. After the linking stage all groups with at least $N_{\rm min}$ are kept and circular velocity profiles are calculated around the center of mass of each group using 100 linear spherical bins. Since 6DFOF finds only the peaks in phase-space density we set the radius of the outermost radial bin to 5 times the half mass radius of the linked group. The steps described above were implemented in parallel within PKDGRAV and they run at with vanishing computational expense compared to the gravity calculations. We omit the computationally expensive step of removing unbound particles and hence we don't actually determine subhalo masses. Instead we estimate $v_{\rm c,max}$ as a proxy for mass by fitting the circular velocity profiles using the circular velocity corresponding to an NFW subhalo embedded in a constant density background. The three free parameters in these fits are $v_{\rm c,max}$ and $r_{\rm v_{c,max}}$ of the subhalo and the background density. We minimize the absolute velocity differences.

Additionally we only allow fits where the subhalo mass enclosed within $r_{\rm v_{c,max}}$ is larger than the background mass. This constraint prevents a few cases (about 2% of the groups) where small fluctuations in the background density at large radii are fitted with an extended, diffuse NFW halo which lies well below the background density at most radii. Figure A10 shows some example circular velocity profiles around 6DFOF-structures found within the virial radius of the $z = 86$ SUSY halo. Typical z=0 subhalos are much denser than the local background and show a clear peak in the total circular velocity profile. Early subhalos, on the other hand, often lack a clearly distinguished peak and appear as excess circular velocity above the linear circular velocity from a constant density background (Figure A10).

After some experimentation we found that with $b = 0.04$, $b_v = 295\ {\rm km\,s^{-1}}$ and $N_{\rm min} = 32$ the SKID subhalo velocity function and radial distribution for the $z = 0$ cluster B9 are almost exactly reproduced. They differ significantly only below about $0.025 v_{\rm c,max,host}$ which lies below the completeness limit of about $0.05 v_{\rm c,max,host}$ in such a simulation (e.g. Ghigna et al. 2000; Diemand et al. 2004; Reed et al. 2005). The 6DFOF results are not sensitive to small (15%) changes in both b and b_v. The adopted velocity linking of $b_v = 295\ {\rm km\,s^{-1}}$ is about four times smaller than the mean 1D velocity dispersion within the virial radius. This suppresses the random links between background particles even in dense regions were each sphere of radius $0.04 \times dx$ contains many particles. Only a prolate structure enclosed in the inner 15 kpc (about 1.5 percent of the virial radius) is linked together. In this paper we don't count this central structure as a subhalo[5].

In the SUSY halo at $z = 86$ we chose a somewhat larger space linking length due to the smaller peak overdensities $b = 0.057$ and rescale the velocity linking lengths to $b_v = 4.15\ {\rm m\,s^{-1}}$ (four times smaller than the mean 1D velocity dispersion within the virial radius) and we keep $N_{\rm min} = 32$. Unfortunately just as with SKID also the 6DFOF subhalo lists at $z = 86$ depend strongly on the choice of group-finding parameters used. A 15 percent increase (or decrease) in both b and b_v yields a very different velocity function, whereas at $z = 0$ our 6DFOF results are unaffected by the same changes in b and b_v (Figure A11). Reducing the 6DFOF linking lengths by 15 percent (a factor of 2.3 in phase-space density threshold) results in 40 percent less subhalos (459 vs. 779) within the virial radius and the resulting subhalo velocity function is about a factor of five lower. Increasing the linking lengths by 15 percent results in an increase of 68 percent in the number of subhalos (1312 vs. 779), but many of them have maximum circular velocities well below $0.3\ {\rm m\,s^{-1}}$, and show no clear subhalo signal in their total circular velocity profile $v_c(r) = \sqrt{v_{\rm c,sub}^2 + v_{\rm c,BG}^2}$. Visual inspection of these small $v_{\rm c,max,sub}$ structures also shows no convincing peak in either real or phase-space density. Only for the highest $v_{\rm c,max,sub}$ structures do the longer linking length results agree with those using our fiducial values of $b = 0.057$ and $b_v = 4.15\ {\rm m\,s^{-1}}$. This strong parameter dependence of 6DFOF results at $z = 86$ is again a consequence of the similar formation times of small mass, high redshift subhalos and hosts which reduces the contrast in phase-space density.

When tracing structures over time we set $b \times dx$ and b_v to constant values in proper coordinates. This corresponds to using the same proper minimum phase-space density to define structures at different epochs. This choice is motivated by the fact that the high (phase-space) density peaks we aim to identify have long decoupled from the Hubble expansion, i.e. they correspond to the inner cores of virialized systems. Employing a constant comoving linking length would result in a decreasing phase-space density threshold. The values we use are $b \times dx = 0.04 \times 0.111\,{\rm kpc} \times 1/(1+0) = 4.444$ proper kpc, $b_v = 295\ {\rm km\,s^{-1}}$ for the B9 cluster and $b \times dx = 0.057 \times 0.3\,{\rm pc} \times 1/(1 + 86.3) = 0.197$ proper Mpc and

[5] SKID produces a similar central object which is always discarded in this work as well.

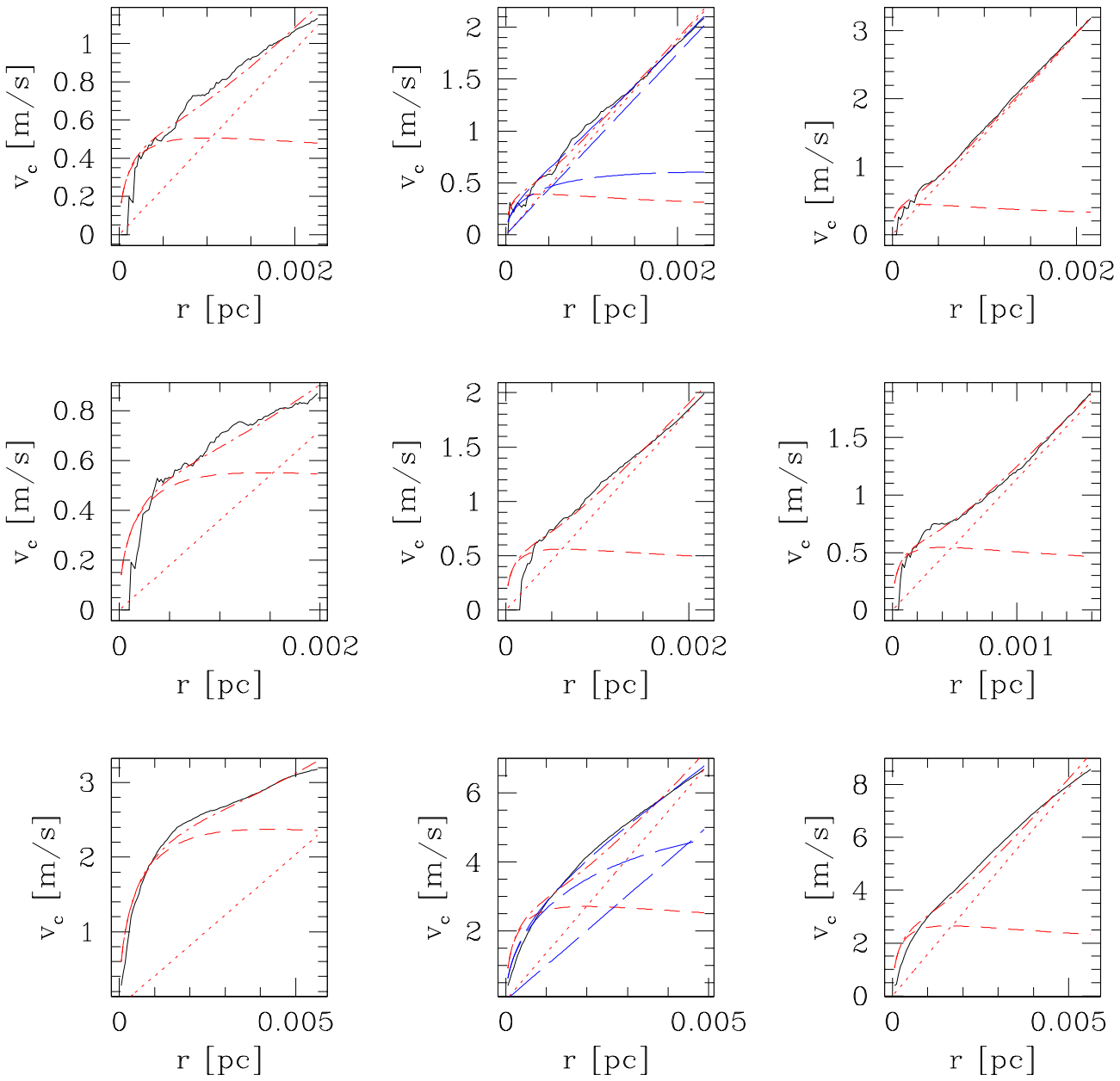

FIG. A10.— Example circular velocity profiles (*solid*) of structures found with 6DFOF within the virial radius of the $z = 86$ SUSY CDM halo. Best fit total circular velocity profiles $v_c(r)$ (*dashed-dotted*) contain a contribution from an NFW subhalo $v_{\rm c,sub}$ (*dashed*) and from a homogeneous background density $v_{\rm c,BG}$ (*dotted*), i.e. $v_c(r) = \sqrt{v_{\rm c,sub}^2 + v_{\rm c,BG}^2}$. Upper panels show small subhalos below the completeness limit of about $0.05 v_{\rm c,max,host} = 1\ {\rm m\,s^{-1}}$ and the lower panels show larger subhalos. From left to right subhalos lie closer to the host center, i.e. the background density increases. In two cases (middle panels of the top and bottom rows) we also show the best fits obtained without the constraint that the subhalo mass must be larger than the background within $r_{\rm v_{c,max}}$ (*long-dashed*). Velocities and radii are given in physical units.

$b_v = 4.15\ {\rm m\,s^{-1}}$ for the SUSY halo.

REFERENCES

Ando, S., & Komatsu, E. 2006, PhRvD, 73, 023521
Berezinsky, V., Dokuchaev, V., & Eroshenko, Y., 2006, PhRvD, 73, 063504
Bertschinger, E. 2001, ApJSS, 137, 1
Bode, P., Ostriker, J. P., & Turok, N. 2001, ApJ, 556, 93
Calcaneo-Roldan, C., & Moore, B. 2000, PhRvD, 62, 123005
Colafrancesco, S., Profumo, S., & Ullio, P. 2005, A&A, in press (astro-ph/057575)

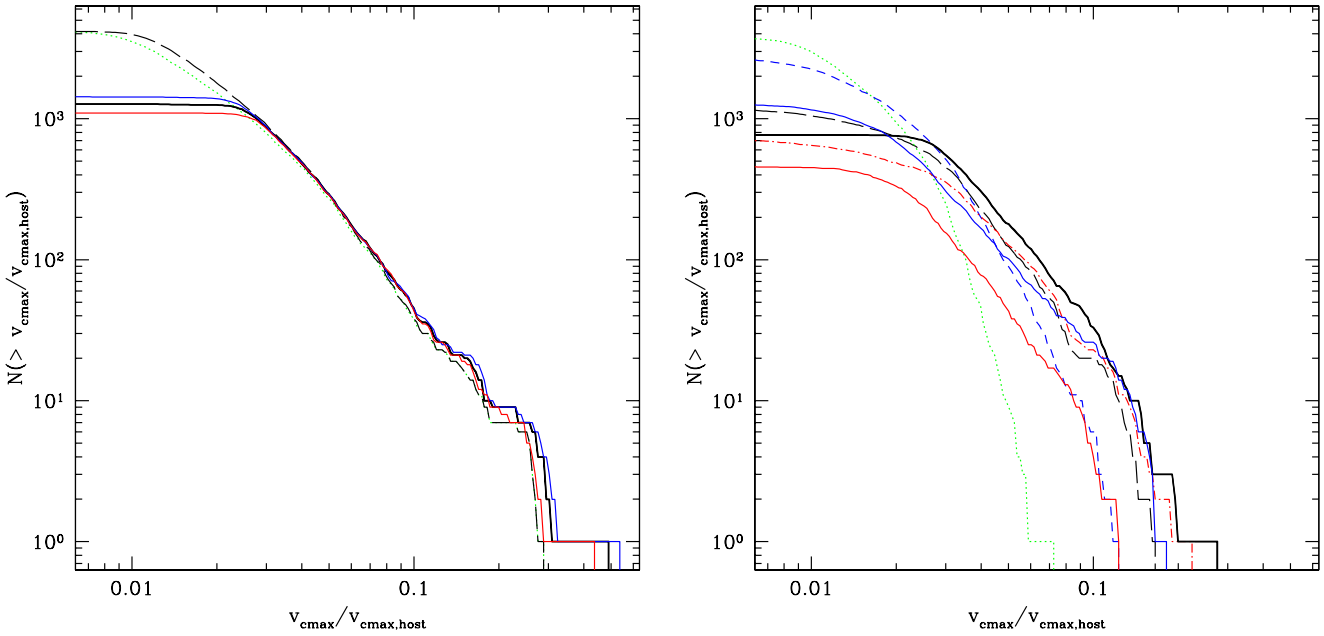

FIG. A11.— SKID and 6DFOF cumulative subhalo velocity functions for the $z = 0$ galaxy cluster (*left*) and the $z = 86$ SUSY CDM halo (*right*). The SKID runs used $N_{\rm min} = 10$ and different numbers of neighbors s for the SPH density calculation: $s = 64$ (*dotted*), $s = 256$ (*short-dashed*, SUSY halo only), $s = 1024$ (*long-dashed*), and $s = 2048$ (*dashed-dotted*, SUSY halo only). The 6DFOF phase-space group finder was run with $b = 0.04$, $b_v = 295$ km s^{-1} and $N_{\rm min} = 32$ (*thick solid*) and 15% larger (upper *solid*) and 15% smaller (*lower solid*) linking lengths $b = 0.04$ and b_v. Varying both linking lengths by 15% corresponds to a factor of difference 1.5 in both real and velocity space minimum densities and to a factor of 2.3 in phase-space density threshold.

Colín, P., Avila-Reese, V.,& Valenzuela, O. 2000, ApJ, 542, 622
Davis, M., & Djorgovski, S., 1985, ApJ, 299, 15
Diemand, J., Moore B., & Stadel, J. 2004, MNRAS, 352, 535
Diemand, J., Moore, B., & Stadel, J. 2004, MNRAS, 353, 624
Diemand, J., Moore B., & Stadel J. 2005, Nature, 433, 389
Gao, L., White, S. D. M., Jenkins, A., Stoehr, F., & Springel, V. 2004, MNRAS, 355, 819
Gao, L., White, S. D. M., Jenkins, A., Frenk, C. S., & Springel, V. 2005, MNRAS, 363, 379
Ghigna, S., Moore, B., Governato, F., Lake, G., Quinn, T., & Stadel, J. 2000, ApJ, 544, 616
Götz, M., & Sommer-Larsen, J. 2003, Ap&SS, 284, 341
Green, A. M., Hofmann, S., & Schwarz, D. J. 2004, MNRAS, 353, L23
Green, A. M., Hofmann, S.,& Schwarz, D. J. 2005, JCAP, 0508, 003
Kazantzidis, S., Mayer, L., Mastropietro, C., Diemand, J., Stadel, J.,& Moore B. 2004, ApJ, 608, 663
Klypin, A., Kravtsov, A. V., Valenzuela, O.,& Prada F. 1999, ApJ, 522, 82
Knebe, A., Devriendt, J. E. G., Gibson, B. K.,& Silk, J. 2003, MNRAS, 345, 1285
Loeb, A., & Zaldarriaga, M. 2005, Phys. Rev. D, 71, 103520
Moore, B., Ghigna, S., Governato, F., Lake, G., Quinn, T., Stadel, J., & Tozzi, P. 1999, ApJ, 524, L19
Moore, B., Calcaneo-Roldan, C., Stadel, J., Quinn, T., Lake, G., Ghigna, S., & Governato, F. 2001, PhRvD, 64, 063508
Mohayaee, R., & Shandarin, S., 2006, MNRAS, 366, 1217
Navarro, J. F., Frenk, C. S., & White, S. D. M. 1997, ApJ, 490, 493
Oda, T., Totani, T., & Nagashima, M. 2005, ApJ, 633, L65
Reed, D., Gardner, J., Quinn, T., Stadel, J., Fardal, M., Lake, G., & Governato, F. 2003, MNRAS, 346, 565
Reed, D., Governato, F., Quinn, T., Gardner, J., Stadel, J., & Lake, G. 2005, MNRAS, 359, 1537
Sheth, R. K., & Tormen, G., 1999, MNRAS, 308, 119
Stadel, J. 2001, PhD thesis, U. Washington
Stoehr, F., White, S. D. M., Springel, Y., Tormen, G., & Yoshida, N. 2003, MNRAS, 345, 1313, (S03)
Taylor, J.E., & Silk, J. 2003, MNRAS, 339, 505
Ullio, P., Bergstrom, L., Edsjo, J., & Lacey C.G. 2002, PhRvD, 66, 123502
Wadsley, J. W., Stadel, J., & Quinn, T. 2004, New Astronomy, 9, 137
White, S. M. D. 1993, in: R. Schaeffer et al. (eds.), Cosmology and Large-Scale Structure: Les Houches, Elsevier, Amsterdam, p. 349-430.
Yoshida, N., Sokasian, A., Hernquist, L., & Springel, V. 2003, ApJ, 591, L1
Zhao, H.S., Taylor, J. E., Silk, J., & Hooper, D. 2005, preprint (astro-ph/0508215)